First Measurement of the Quadrupole Moment of the 2_1^+ State in ^{110}Sn

J. Park,[1,2,*,†] R. A. Lopez,[1] J. Cederkall,[1,3,‡] C. Fahlander,[1] P. Golubev,[1] A. Knyazev,[1] E. Rickert,[1] J. Iwanicki,[4] K. Wrzosek-Lipska,[4] A. Blazhev,[5] P. Reiter,[5] D. Rosiak,[5] M. Seidlitz,[5] N. Warr,[5] P. A. Butler,[6] L. P. Gaffney,[6] T. Berry,[7] D. M. Cox,[8,9] J. Pakarinen,[8,9] Th. Kröll,[10] C. Henrich,[10] M. Schilling,[10] C. Stahl,[10] M. von Schmid,[10] G. Rainovski,[11] C. Berger,[12] C. Berner,[12] R. Gernhäuser,[12] A. Illana,[8,13,14,§] H. De Witte,[13] M. Górska,[15] T. Habermann,[15] S. Saha,[15] G. de Angelis,[14] M. J. G. Borge,[3,16] O. Tengblad,[16] T. Otsuka,[17,18] and Y. Tsunoda[19]

[1]*Department of Physics, Lund University, Box 118, SE-221 00 Lund, Sweden*
[2]*Center for Exotic Nuclear Studies, Institute for Basic Science (IBS), Daejeon 34126, Republic of Korea*
[3]*CERN, CH-1211 Geneva 23, Switzerland*
[4]*Heavy Ion Laboratory, University of Warsaw, PL-02-093 Warsaw, Poland*
[5]*Institut für Kernphysik, Universität zu Köln, D-50937 Köln, Germany*
[6]*Oliver Lodge Laboratory, University of Liverpool, Liverpool, United Kingdom*
[7]*Department of Physics, University of Surrey, Guildford, Surrey GU2 7XH, United Kingdom*
[8]*Accelerator Laboratory, Department of Physics, University of Jyväskylä, FI-40014 Jyväskylä, Finland*
[9]*Helsinki Institute of Physics, University of Helsinki, P.O. Box 64, FI-00014 Helsinki, Finland*
[10]*Institut für Kernphysik, Technische Universität Darmstadt, D-64289 Darmstadt, Germany*
[11]*Faculty of Physics, Sofia University, 1164 Sofia, Bulgaria*
[12]*Physik Department, Technische Universität München, D-85748 Garching, Germany*
[13]*KU Leuven, Instituut voor Kern- en Stralingsfysica, B-3001 Leuven, Belgium*
[14]*Istituto Nazionale di Fisica Nucleare, Laboratori Nazionali di Legnaro, I-35020 Legnaro, Italy*
[15]*GSI Helmholtzzentrum für Schwerionenforschung GmbH, D-64291 Darmstadt, Germany*
[16]*Instituto de Estructura de la Materia, CSIC, E-28006 Madrid, Spain*
[17]*Department of Physics, The University of Tokyo, 7-3-1 Hongo, Bunkyo, Tokyo 113-0033, Japan*
[18]*RIKEN Nishina Center, 2-1 Hirosawa, Wako, Saitama 351-0198, Japan*
[19]*Center for Nuclear Study, The University of Tokyo, 7-3-1 Hongo, Bunkyo, Tokyo 113-0033, Japan*

(Received 28 February 2025; revised 14 July 2025; accepted 20 October 2025; published 25 November 2025)

The Sn isotopic chain, exhibiting double shell closures at ^{100}Sn and ^{132}Sn, is a key testing ground for theoretical models of the atomic nucleus. It was originally predicted that the transitional matrix elements between the first 2^+ state and the 0^+ ground state for the even-even isotopes in this chain should show a simple dependence on the neutron number. This prediction was, however, disproven experimentally in some of the first experiments with postaccelerated radioactive beams, a situation that has remained unresolved ever since. Subsequent theoretical work has suggested that the explanation can be found in proton excitations across the $Z = 50$ shell gap, with an accompanying experimental signature that the first excited 2^+ state in ^{110}Sn should have a distinct oblate shape. In this Letter, we present the first measurements of the spectroscopic quadrupole moment of the 2_1^+ state, $B(E2; 4_1^+ \to 2_1^+)$ and $B(E2; 4_2^+ \to 2_1^+)$ values for ^{110}Sn, as well as the $B(E2; 2_1^+ \to 0_1^+)$ value with significantly improved precision compared to previous results. From the same experiment, half-lives of the 2_1^+ and 4_1^+ states were measured using the Doppler shift attenuation method. Our combined result, $Q(2_1^+) = 20(8)$ efm^2 for ^{110}Sn, is the largest positive value known among the Sn isotopes, indicating an oblate shape of the state by more than 2σ. Comparison of the $E2$ transition strengths and quadrupole moments with recent shell model calculations are presented.

DOI: 10.1103/7ysn-8y1w

*Contact author: jcpark@ibs.re.kr
†Present address: Physics Department, Hope College, Holland, Michigan 49423, USA.
‡Contact author: joakim.cederkall@fysik.lu.se
§Present address: Grupo de Física Nuclear, EMFTEL, and IPARCOS, Universidad Complutense de Madrid, 28040 Madrid, Spain.

Among the several thousands of nuclear systems that exist within the nuclear drip lines, only a few isotopes exhibit shell closures for both neutrons and protons. These isotopes, called doubly magic, are cornerstones for nuclear theory, as they provide experimental benchmarks for the nuclear shell model and, consequently, for models of the strong interaction in the nuclear medium. Two of these isotopes, ^{100}Sn and ^{132}Sn, are especially interesting as they are the end points of the longest magic isotopic chain available in nature, spanning neutron numbers from $N = 50$ to $N = 82$.

However, nuclear models have had only limited success in reproducing a fundamental observable in this chain: the reduced transition probability $B(E2)$ between the 0^+ ground state and the first excited 2^+ state in the even-A isotopes [1–5]. This has remained a puzzle ever since the first measurements of this quantity could be carried out in the neutron-deficient Sn isotopes [6–40].

To first approximation, the 2_1^+ state in the even-A Sn isotopes is predicted to consist of a broken neutron pair coupled to a spin of $2\hbar$ [41]. In the same manner, it is predicted that the energy of the 2^+ state should remain constant over the chain and that the $B(E2; 2_1^+ \rightarrow 0_1^+)$ values should exhibit a simple dependence on the neutron occupation number in the major shell. However, experiments have shown that the measured $B(E2; 2_1^+ \rightarrow 0_1^+)$ values in the lighter even-even Sn isotopes ($A < 116$) are consistently higher than predicted, also when compared to more advanced large-scale shell model (LSSM) calculations.

This situation has prompted many theoretical attempts to reproduce the $B(E2; 2_1^+ \rightarrow 0_1^+)$ trend [5,42–53]. In a relatively recent Letter, Togashi *et al.* [5] presented Monte Carlo shell model (MCSM) calculations that attribute the observed effect to proton excitations from the $1g_{9/2}$ to the $1g_{7/2}$ orbit, across the $Z = 50$ shell gap. The same work also predicts that the proton-core excitation component of the 2_1^+-state wave function reaches a maximum for ^{110}Sn and that a shape change occurs for the 2_1^+ state, from a prolate shape in ^{108}Sn to a distinct oblate shape in ^{110}Sn.

To address this question experimentally, we present the first measurement of the spectroscopic quadrupole moment of the 2_1^+ state, $Q(2_1^+)$, in ^{110}Sn via Coulomb excitation, together with $B(E2)$ measurements for the $2_1^+ \rightarrow 4_1^+$ and $2_1^+ \rightarrow 4_2^+$ transitions. We also give a high-precision result for the $B(E2)$ of the $0_1^+ \rightarrow 2_1^+$ excitation taking these higher-order effects into account. Furthermore, we provide half-lives measured via the Doppler shift attenuation method (DSAM) in the same experiment. The new results are compared to shell-model (SM) predictions, including the above-mentioned MCSM approach. This study, of higher-order excitation effects in the neutron-deficient Sn isotopes, was possible due to the new and unique capabilities at CERN-ISOLDE to deliver high-intensity, high-quality radioactive beams of sufficient energy to use high-Z targets, in this case ^{206}Pb.

The experiment was carried out at the HIE-ISOLDE facility [54] at CERN using the Miniball spectrometer [55] for γ-ray detection. The beam of radioactive ^{110}Sn was produced by bombarding a thick lanthanum carbide (LaC_x) target with the 1.4-GeV protons from the CERN PS booster. The purity of the beam was enhanced to 98(1)% using the ISOLDE resonance ionization laser ion source [56]. The ^{110}Sn beam, with an average intensity of 1×10^7 particles per second, was postaccelerated to 4.4 MeV/nucleon before impinging on a 4-mg/cm^2 ^{206}Pb target. The beam energy satisfied the "safe" energy criterion [57] for the ^{110}Sn-^{206}Pb projectile-target pair at all scattering angles.

The energy and scattering angle of the ^{110}Sn and the ^{206}Pb nuclei were measured using a circular double-sided silicon strip detector with four quadrants [58], having a polar angle coverage of $\theta_{lab} = 21.4°$–$60.8°$. The Miniball γ-ray spectrometer, which is an array of segmented high-purity germanium (HPGe) crystals, was energy and efficiency calibrated using standard radioactive sources of ^{152}Eu, ^{133}Ba, and ^{60}Co, while the Si detector was calibrated using a ^{239}Pu-^{241}Am-^{244}Cm α source.

The γ-ray energy spectra, corrected for Doppler shifts for the ^{110}Sn beam or the ^{206}Pb target nuclei, are shown in Fig. 1. Two γ rays were found in γ-γ coincidence with the 1212-keV, $2_1^+ \rightarrow 0^+$ transition in ^{110}Sn. The 985-keV γ ray from the 4_1^+ state in ^{110}Sn was observed in the single spectrum and confirmed in γ-γ coincidence. Furthermore, a peak was observed around 1245 keV that could correspond to the 1243-keV γ ray depopulating the 4_2^+ state or the 1246-keV γ ray from the 3_1^- state. The latter was ruled out

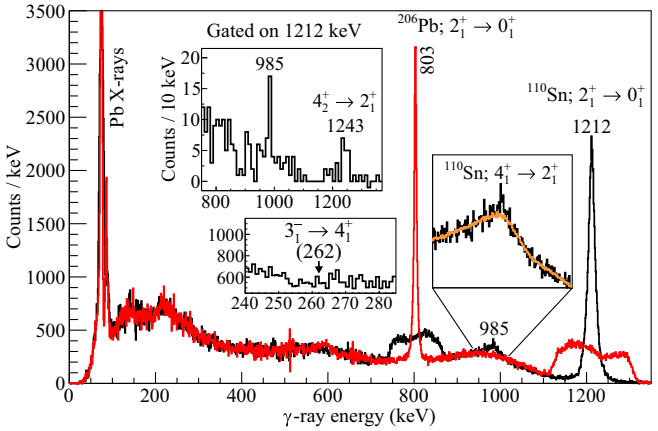

FIG. 1. Doppler-corrected γ-ray energy spectra: on ^{110}Sn kinematics (black) and on ^{206}Pb kinematics (red). The γ-γ coincidence projection of the 1212-keV gate in ^{110}Sn is shown in the top left inset. The right inset corresponds to the single spectrum enlarged on the 985-keV peak against the simulated background spectrum (orange) assuming only the 1212-keV γ-ray emission. The bottom left inset demonstrates no signature of 262-keV γ ray from the 3_1^- state.

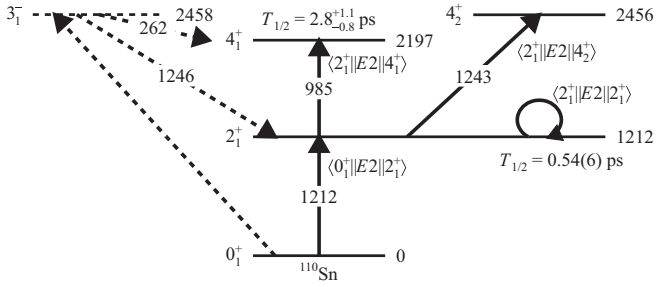

FIG. 2. Partial level scheme, electromagnetic transition matrix elements, and the measured half-lives of the 2_1^+ and 4_1^+ states of ^{110}Sn in this Letter. Coulomb excitation to the 3_1^- state was not observed with statistical significance. The transition energies are given in keV.

due to the nonobservation of the 262-keV γ-ray side branch that feeds the 4_1^+ state from the 3_1^- state. To investigate a hypothetical Coulomb excitation of the 3_1^- state, an upper limit on the intensity of the nonobserved 262-keV γ ray was deduced from the spectrum shown in the inset in Fig. 1. The result of that analysis is discussed in End Matter. The level scheme of interest for ^{110}Sn in this Letter is shown in Fig. 2.

The collected γ-ray statistics allowed for divisions of the γ-ray yield data for the 2_1^+ states of both ^{110}Sn and ^{206}Pb into five subsets corresponding to different scattering angles of the ^{110}Sn ions (see Table I). This angular subdivision is of key importance to constrain the $\langle 0_1^+||E2||2_1^+\rangle$ and $\langle 2_1^+||E2||2_1^+\rangle$ matrix elements in the analysis. The total yield uncertainty was 5% for each dataset. The data analysis was done using the semiclassical Coulomb excitation code GOSIA [59–62].

Two separate normalizations were used for the γ-ray yields when determining the $B(E2; 2_1^+ \rightarrow 0_1^+)$ and $Q(2_1^+)$ of ^{110}Sn. In the first case, the γ-ray yields of both the ^{110}Sn and ^{206}Pb nuclei were analyzed using an iterative analysis method as described by Zielińska *et al.* (see Sec. 4.4.2 in Ref. [63]) following previous Coulomb excitation experiments at HIE-ISOLDE [64–66]. The result is a χ^2 surface (normalized to the number of degrees of freedom) calculated over a grid of $\langle 0_1^+||E2||2_1^+\rangle$ and $\langle 2_1^+||E2||2_1^+\rangle$ values

TABLE I. Subdivisions of γ-ray yield data for GOSIA analysis according to ^{110}Sn scattering angles. For high laboratory angles which were not covered by the silicon detector, the scattering angle of ^{110}Sn was derived from the kinematics of the detected target nucleus ^{206}Pb.

Detected particle	θ_{lab} (^{110}Sn)	θ_{cm} (^{110}Sn)
^{110}Sn	21.4°–36.4°	32.2°–54.3°
^{110}Sn	36.6°–47.4°	54.5°–69.9°
^{110}Sn	47.5°–55.1°	70.1°–80.6°
^{206}Pb	57.9°–75.3°	86.0°–107.6°
^{206}Pb	75.4°–106.0°	108.0°–137.7°

where the minimum χ^2 corresponds to the optimal values for these two parameters. The resulting surface is shown in the top panel in Fig. 3, while the matrix elements are listed in the middle column in Table II. A quadrupole moment, $Q(2_1^+) = 17^{+10}_{-8}$ efm^2, results from this analysis.

The second normalization method involved half-life measurement of the 2_1^+ excited state ^{110}Sn, where the resulting $T_{1/2}$ value served as absolute normalization parameter of the Coulomb excitation γ-ray yields. This could be accomplished as a fraction of events resulted in either the beam or target nucleus being Coulomb excited and scattered so that it was significantly slowed down or stopped inside the ^{206}Pb target before γ-ray emission, resulting in a half-life-dependent γ-ray line shape. The line shape was simulated for different half-lives of the relevant states using the Geant4 framework [67–69]. The half-lives extracted for the 2_1^+ and 4_1^+ states from the simulation are 0.54(6) and $2.8^{+1.1}_{-0.8}$ ps, respectively (see Figs. 4 and 5). These values are consistent with $T_{1/2}(2_1^+) = 0.56(7)$ ps and $T_{1/2}(4_1^+) > 2.77$ ps from a previous experiment [30]. Using the two half-lives measured in this Letter to constrain the fit gives $Q(2_1^+) = 11^{+6}_{-5}$ efm^2. The corresponding matrix element is marked by the open square in

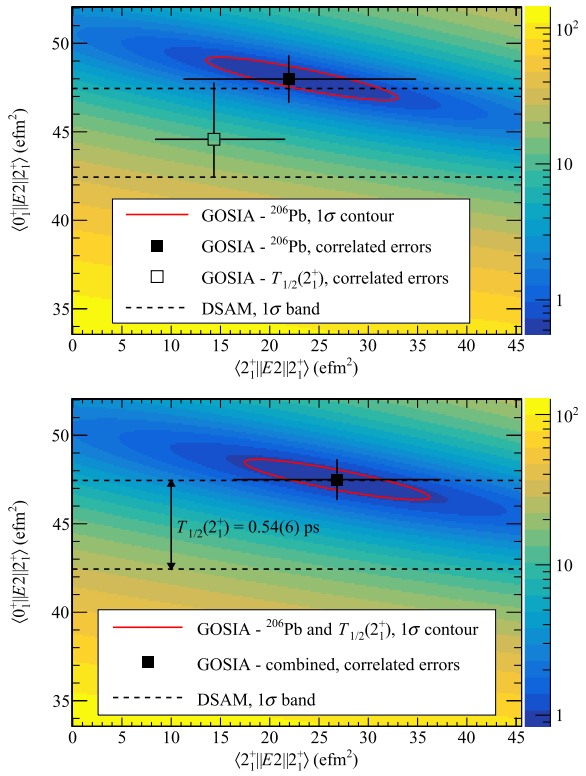

FIG. 3. Map of normalized χ^2 values from GOSIA as a function of the $\langle 2_1^+||E2||2_1^+\rangle$ and $\langle 0_1^+||E2||2_1^+\rangle$ matrix elements of ^{110}Sn. Top: Results from the iterative method using two separate normalization schemes. Bottom: The χ^2 map after combining with the $T_{1/2}(2_1^+)$ result from this Letter. See the text for details.

TABLE II. Experimental $E2$ matrix elements of ^{110}Sn from GOSIA, based on two normalization schemes of the γ-ray yield data.

Matrix element (in efm^2)	N [^{206}Pb]	N [$T_{1/2}(2_1^+, 4_1^+)$]
$\langle 0_1^+ \|\| E2 \|\| 2_1^+ \rangle$	48.0(13)	$44.6^{+3.2}_{-2.1}$
$\langle 2_1^+ \|\| E2 \|\| 2_1^+ \rangle$	22^{+13}_{-11}	14^{+7}_{-6}
$\langle 2_1^+ \|\| E2 \|\| 4_1^+ \rangle$	51^{+10}_{-7}	51^{+9}_{-7}
$\langle 2_1^+ \|\| E2 \|\| 4_2^+ \rangle$	50^{+9}_{-12}	49^{+8}_{-11}

the top panel in Fig. 3. For the two 4^+ states, the $B(E2; 4_1^+ \to 2_1^+)$ and $B(E2; 4_2^+ \to 2_1^+)$ values are 290^{+100}_{-80} e^2 fm^4 and 260^{+80}_{-120} e^2 fm^4, respectively (see also the right column in Table II). Further details are given in End Matter.

The $B(E2)$ and $Q(2_1^+)$ values from the analyses are listed in Table III. The χ^2 surface in the top panel in Fig. 3 was also combined with a χ^2 map derived from the $T_{1/2}(2_1^+)$ result in order to obtain a cumulative $\chi^2_{\min}$ from both methods, with the assumption that the γ-ray intensities used for cross sections and the γ-ray line shape analysis are only weakly correlated. The minimum χ^2 value from this combined approach, shown in the bottom panel in Fig. 3, is located at $\langle 0_1^+ \|\| E2 \|\| 2_1^+ \rangle = 47.5(12)$ efm^2 and $\langle 2_1^+ \|\| E2 \|\| 2_1^+ \rangle = 27(11)$ efm^2. From these, we obtain $B(E2; 2_1^+ \to 0_1^+) = 451(22)\,\text{e}^2\,\text{fm}^4$ and $Q(2_1^+) = 20(8)\,\text{efm}^2$. The $B(E2; 2_1^+ \to 0_1^+)$ is in agreement with the results of the two previous Coulomb excitation experiments [1,2] but significantly more precise. Consequently, after taking into account the nonzero $Q(2_1^+)$ and excitations to the two 4^+ states, the observed $B(E2; 2_1^+ \to 0_1^+)$ in ^{110}Sn still deviates from previous predictions made with state-of-the-art LSSM calculations [1,2].

In the following, the new quadrupole moment $Q(2_1^+)$ and the $B(E2)$ values from this Letter are compared with the predictions of three theoretical models. First, the SR88MHJM model [71], which has been used recently to interpret spectroscopic quantities in nuclei close to ^{100}Sn [72–76], is included as a representation of a traditional SM calculation. This model adopts a G-matrix approach based on a CD-Bonn potential and assumes a core of ^{88}Sr with a valence model space up to the next major shells at $Z = 50$ and $N = 82$. More details are given in Refs. [77,78]. The deviation between our combined result and this model in $B(E2; 2_1^+ \to 0_1^+)$ for ^{110}Sn is more than 3σ, which highlights the limitations of the model using only valence neutrons to account for the quadrupole strength. This conclusion is, however, at odds with a previous g-factor and half-life measurement on ^{110}Sn [30], that concluded that excitations of the $Z = 50$ core was not required. Regarding these earlier findings, it should be noted that the half-life-based $B(E2; 2_1^+ \to 0_1^+)$ was ≈20% lower than literature values from Coulomb excitation and that the uncertainties on the g factors of the 2_1^+, 4_1^+, and 6_1^+ states were at minimum 38%. In another theoretical approach, the pairing-quadrupole interplay in the Cd and Sn isotopes was investigated by Zuker [53]. This model, named "I.3.4," adopts $V_{\text{low-}k}$ variants [79] of the N3LO interaction [80] with replacements of the monopole part for ^{100}Sn from Ref. [81] and enhancements of the quadrupole and pairing components of a phenomenological SM by 30% [82] and 40% [82,83], respectively. Here, the model space of the interaction is limited to the neutron gds orbits above $N = 50$. The I.3.4 model has been particularly effective in reproducing the experimental $B(E2; 2_1^+ \to 0_1^+)$ and

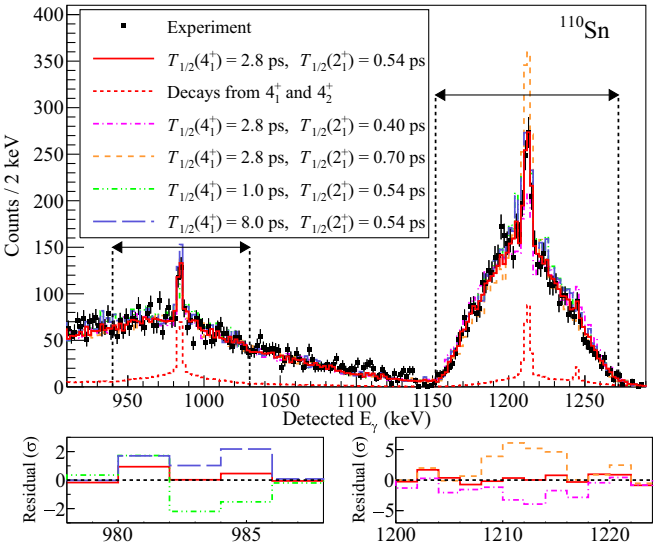

FIG. 4. Experimental (black points) and simulated (histograms) γ-ray energy spectra without Doppler correction. The bottom two panels show the weighted residuals around the stopped γ-ray peaks. See End Matter for details.

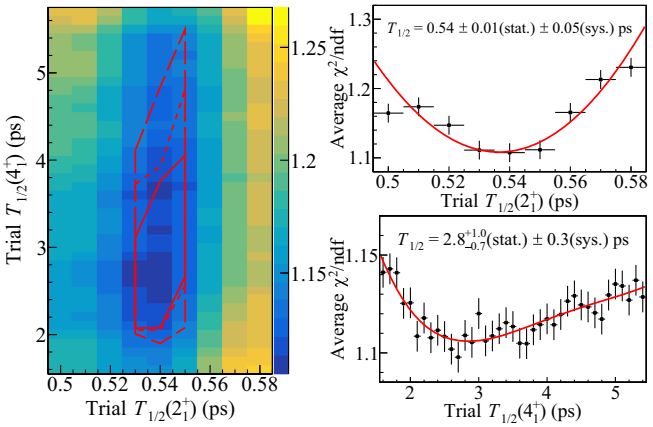

FIG. 5. Left: normalized χ^2 map of γ-ray spectrum comparisons between the experiment and simulations as shown in Fig. 3, as a function of the trial half-lives of the 4_1^+ and 2_1^+ states. Right: 1D χ^2 projections in trial $T_{1/2}$ for the 2_1^+ state (top) and the 4_1^+ state (bottom). See End Matter for details.

TABLE III. Reduced $E2$ transition strengths and spectroscopic quadrupole moment determined in this Letter. The theoretical values from three SM interactions and their effective charges are listed for comparison. The proton effective charge for SR88MHJM is omitted, since their proton model space is limited to $38 \leq Z \leq 50$.

Observable	Experiment					Theory, (e_π, e_ν) [in e]		
$B(E2)$ in e^2 fm^4, $Q(2_1^+)$ in efm^2	N [^{206}Pb]	From GOSIA N [$T_{1/2}(2_1^+)$]	Combined	From DSAM $T_{1/2}$	Literature	SR88MHJM [71] $(x, 1.0)$	I.3.4 [53] (1.4,0.72)	MCSM [70] (1.25,0.75)
$B(E2; 2_1^+ \to 0_1^+)$	460(26)	397^{+57}_{-38}	451(22)	400^{+50}_{-40}	440(44) [1], 480(64) [2], 388(48) [30]	367	456	469
$B(E2; 4_1^+ \to 2_1^+)$	290^{+110}_{-90}	290^{+100}_{-80}	300(100)	220^{+90}_{-60}	< 221[a] [30]	77	297	956
$B(E2; 4_2^+ \to 2_1^+)$	280^{+90}_{-130}	260^{+80}_{-120}	260(120)			296		47
$Q(2_1^+)$	17^{+10}_{-8}	11^{+6}_{-5}	20(8)			−5	3	38

[a]From $T_{1/2}(4_1^+) > 2.77$ ps [30].

$B(E2; 4_1^+ \to 2_1^+)$ trends in the light Sn isotopes [37], but calculations for the heavier Sn isotopes have not yet been presented. Finally, the model space of the MCSM, mentioned in the Introduction and presented in Ref. [5], includes the orbits in the *gds* harmonic oscillator shell as well as the *hfp* orbits for both protons and neutrons above a ^{80}Zr core. The large model space was accounted for by employing the MCSM as described in Refs. [84,85]. The effective interaction parameters were adopted from the JUN45 [86] and SNBG3 [87] models.

Referring to Table III for comparison, both the I.3.4 and MCSM models are in better agreement with the experimental $B(E2; 2_1^+ \to 0_1^+)$ values of the light Sn isotopes than SR88MHJM.

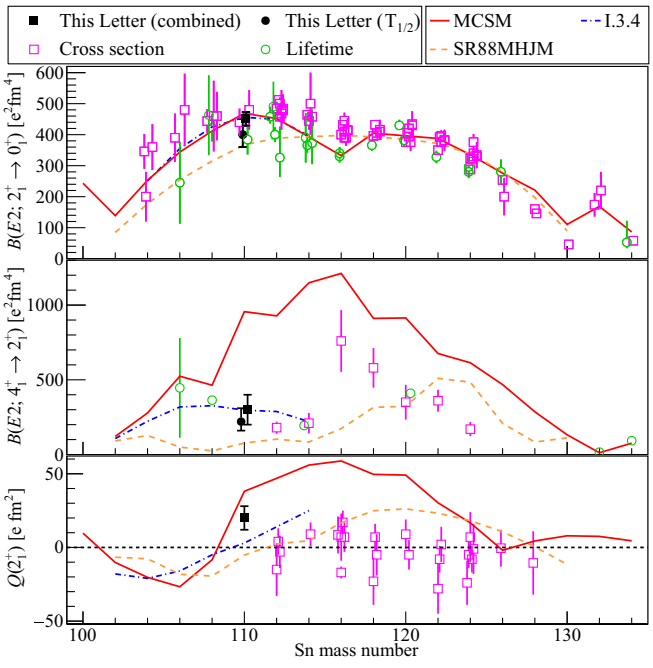

FIG. 6. Electric quadrupole transition strengths [top, $B(E2; 2_1^+ \to 0_1^+)$; middle, $B(E2; 4_1^+ \to 2_1^+)$] and spectroscopic quadrupole moment $Q(2_1^+)$ (bottom) of the Sn isotopes. The MCSM results were taken from Refs. [5,70], and the SR88MHJM results were provided by Ref. [71]. The experimental values are taken from Refs. [1–4,6–9,11–18,20–22,24,26,27,29–40,88].

The systematics of the electric quadrupole moments in the Sn isotopes are shown in Fig. 6. For several even-even Sn isotopes, excitation cross-section experiments have yielded higher magnitudes of matrix elements for the 2_1^+ state compared to those obtained via $T_{1/2}(2_1^+)$ measurements (see top panel in Fig. 6). Although the latest DSAM results for stable ^{112,120}Sn [35,38] hint at some reconciliation with the cross-section measurements, we suggest that additional DSAM experiments with isotopically enriched targets are carried out to study this question further. The central panel in Fig. 6 shows the trend of the $B(E2; 4_1^+ \to 2_1^+)$ values in the Sn chain. None of the available models reproduces the abrupt increase in the $B(E2; 4_1^+ \to 2_1^+)$ values that is observed between ^{114}Sn and ^{116}Sn. The MCSM model shows an increasing trend when the $N = 66$ neutron midshell is approached from either direction and overpredicts $B(E2; 4_1^+ \to 2_1^+)$ of ^{110}Sn from our measurement significantly. In contrast, the I.3.4 model is consistent with the results of the current Letter and also reproduces the general trend of $B(E2; 2_1^+ \to 0_1^+)$ and $B(E2; 4_1^+ \to 2_1^+)$ values of the lighter isotopes relatively well. The treatment of pairing in this model has been given as the reason for its success despite the limited model space. For the $Q(2_1^+)$ trend, all three models predict a change from prolate to oblate shapes of the 2_1^+ state in the light isotopes but for different mass numbers. Specifically for ^{110}Sn, the SR88MHJM model predicts a prolate shape, while the I.3.4 and MCSM predict an oblate shape. However, both of these models, with correct signs of $Q(2_1^+)$, show a $\sim 2\sigma$ deviation from our combined result. From the bottom panel in Fig. 6, it is clear that the previously measured $Q(2_1^+)$ values for all isotopes heavier than ^{110}Sn are markedly ambiguous as to their signs and magnitudes. With both theoretical and experimental advances shown here, the popular paradigm of near-zero $Q(2_1^+)$ of the magic Sn isotopes should be rigorously investigated experimentally in order to properly test theoretical predictions for these relatively simple excitations.

In summary, we have presented results from a new high-statistics multistep Coulomb excitation experiment of

^{110}Sn at HIE-ISOLDE. The measured $B(E2;2_1^+ \to 0_1^+) = 451(22)\ e^2\,fm^4$ is the most precise value to date. The $B(E2\downarrow)$ values for the 4_1^+ and 4_2^+ states in ^{110}Sn were determined to be $300(100)\ e^2\,fm^4$ and $260(120)\ e^2\,fm^4$, respectively. In addition, in a combined analysis the $Q(2_1^+)$ of ^{110}Sn was determined as $20(8)\ efm^2$. We conclude that, after including higher-order excitation effects in the analysis, the $B(E2;2_1^+ \to 0_1^+)$ value in ^{110}Sn still deviates from state-of-the-art LSSM predictions but that the observed distinct oblate shape of the 2_1^+ state agrees with both a recent MCSM calculation and a shell model specifically developed to investigate pairing-quadrupole effects in Cd and Sn isotopes.

Acknowledgments—The authors thank the personnel at ISOLDE for producing an intense radioactive beam with high purity, as well as the Miniball Collaboration for their expertise and support. J. Snäll, Lund university, is acknowledged for participating in the first exploratory work with the dataset. This work was supported by the Swedish Research Council under Grants No. 2021-00174-VR, No. 2021-04575-VR, No. 2017-00637-VR, and No. 2017-03986-VR, by the Institute for Basic Science, Republic of Korea, under Grant No. IBS-R031-D1, and the European Union's Horizon Europe Framework research and innovation program under Grant Agreement No. 101057511. G. R. acknowledges the support of the Bulgarian Ministry of Education and Science within the National Roadmap for Research Infrastructures (object CERN). N. W. and P. R. acknowledge the German BMBF under Contracts No. 05P21PKCI1, No. 05P24PCKI1, and No. 05P21RDCI2 and Verbundprojekt No. 05P2021. R. G. acknowledges German BMBF under Grant No. 05P15WOCIA. Funding was also provided by the German BMBF under Contract No. 05P15RDCIA. J. P. and D. M. C. acknowledge the Academy of Finland Project No. 349128. The support of the Polish Ministry of Education and Science under Contract No. 2021/WK/07 is acknowledged. This work was supported in part by HPCI Strategic Program (No. hp150224), also in part by MEXT and JICFuS and a priority issue (Elucidation of the fundamental laws and evolution of the universe) to be tackled by using the Post-"K" Computer (No. hp160211 and No. hp170230), as well as in part by the HPCI system research project (No. hp170182), and by CNS-RIKEN joint project for large-scale nuclear structure calculations.

Data availability—The data are not publicly available. The data are available from the authors upon reasonable request.

[1] J. Cederkäll *et al.*, Phys. Rev. Lett. **98**, 172501 (2007).
[2] C. Vaman *et al.*, Phys. Rev. Lett. **99**, 162501 (2007).
[3] A. Ekström *et al.*, Phys. Rev. Lett. **101**, 012502 (2008).
[4] G. Guastalla *et al.*, Phys. Rev. Lett. **110**, 172501 (2013).
[5] T. Togashi, Y. Tsunoda, T. Otsuka, and M. Honma, Phys. Rev. Lett. **121**, 062501 (2018).
[6] A. M. Kleinfeld, R. Covello-Moro, H. Ogata, G. G. Seaman, S. G. Steadman, and J. De Boer, Nucl. Phys. **A154**, 499 (1970).
[7] P. H. Stelson, F. K. McGowan, R. L. Robinson, and W. T. Milner, Phys. Rev. C **2**, 2015 (1970).
[8] R. Graetzer, S. M. Cohick, and J. X. Saladin, Phys. Rev. C **12**, 1462 (1975).
[9] J. W. Lightbody, S. Penner, S. P. Fivozinsky, P. L. Hallowell, and H. Crannell, Phys. Rev. C **14**, 952 (1976).
[10] M. Hass, C. Broude, Y. Niv, and A. Zemel, Phys. Rev. C **22**, 97 (1980).
[11] N.-G. Jonsson, A. Bäcklin, J. Kantele, R. Julin, M. Luontama, and A. Passoja, Nucl. Phys. **A371**, 333 (1981).
[12] J. Gableske *et al.*, Nucl. Phys. **A691**, 551 (2001).
[13] D. C. Radford *et al.*, Nucl. Phys. **A746**, 83 (2004).
[14] D. C. Radford *et al.*, Nucl. Phys. **A752**, 264 (2005).
[15] A. Banu *et al.*, Phys. Rev. C **72**, 061305(R) (2005).
[16] J. N. Orce, S. N. Choudry, B. Crider, E. Elhami, S. Mukhopadhyay, M. Scheck, M. T. McEllistrem, and S. W. Yates, Phys. Rev. C **76**, 021302(R) (2007).
[17] J. N. Orce *et al.*, Phys. Rev. C **77**, 029902 (2008).
[18] P. Doornenbal *et al.*, Phys. Rev. C **78**, 031303(R) (2008).
[19] M. C. East, A. E. Stuchbery, A. N. Wilson, P. M. Davidson, T. Kibédi, and A. I. Levon, Phys. Lett. B **665**, 147 (2008).
[20] R. Kumar *et al.*, Phys. Rev. C **81**, 024306 (2010).
[21] A. Jungclaus *et al.*, Phys. Lett. B **695**, 110 (2011).
[22] J. M. Allmond *et al.*, Phys. Rev. C **84**, 061303(R) (2011).
[23] J. Walker *et al.*, Phys. Rev. C **84**, 014319 (2011).
[24] G. J. Kumbartzki *et al.*, Phys. Rev. C **86**, 034319 (2012).
[25] J. M. Allmond *et al.*, Phys. Rev. C **87**, 054325 (2013).
[26] V. M. Bader *et al.*, Phys. Rev. C **88**, 051301(R) (2013).
[27] P. Doornenbal *et al.*, Phys. Rev. C **90**, 061302(R) (2014).
[28] A. Corsi *et al.*, Phys. Lett. B **743**, 451 (2015).
[29] J. M. Allmond *et al.*, Phys. Rev. C **92**, 041303(R) (2015).
[30] G. J. Kumbartzki *et al.*, Phys. Rev. C **93**, 044316 (2016).
[31] R. Kumar *et al.*, Phys. Rev. C **96**, 054318 (2017).
[32] M. Spieker, P. Petkov, E. Litvinova, C. Müller-Gatermann, S. G. Pickstone, S. Prill, P. Scholz, and A. Zilges, Phys. Rev. C **97**, 054319 (2018).
[33] D. Rosiak *et al.*, Phys. Rev. Lett. **121**, 252501 (2018).
[34] A. Kundu, S. Santra, A. Pal, D. Chattopadhyay, R. Tripathi, B. J. Roy, T. N. Nag, B. K. Nayak, A. Saxena, and S. Kailas, Phys. Rev. C **99**, 034609 (2019).
[35] A. Kundu *et al.*, Phys. Rev. C **100**, 034327 (2019).
[36] A. Kundu, S. Santra, A. Pal, D. Chattopadhyay, T. N. Nag, R. Gandhi, P. C. Rout, B. J. Roy, B. K. Nayak, and S. Kailas, Phys. Rev. C **100**, 024614 (2019).
[37] M. Siciliano *et al.*, Phys. Lett. B **806**, 135474 (2020).
[38] A. Kundu *et al.*, Phys. Rev. C **103**, 034315 (2021).
[39] M. Piersa-Siłkowska *et al.*, Phys. Rev. C **104**, 044328 (2021).
[40] M. Beuschlein *et al.*, Phys. Rev. C **110**, 054304 (2024).
[41] I. Talmi, Nucl. Phys. **A172**, 1 (1971).
[42] B. A. Brown, N. J. Stone, J. R. Stone, I. S. Towner, and M. Hjorth-Jensen, Phys. Rev. C **71**, 044317 (2005).

[43] A. Ansari, Phys. Lett. B **623**, 37 (2005).
[44] A. Ansari and P. Ring, Phys. Lett. B **649**, 128 (2007).
[45] L. Y. Jia, H. Zhang, and Y. M. Zhao, Phys. Rev. C **75**, 034307 (2007).
[46] I. O. Morales, P. Van Isacker, and I. Talmi, Phys. Lett. B **703**, 606 (2011).
[47] N. Lo Iudice, C. Stoyanov, and D. Tarpanov, Phys. Rev. C **84**, 044314 (2011).
[48] D. Voitenkov, S. Kamerdzhiev, S. Krewald, E. E. Saperstein, and S. V. Tolokonnikov, Phys. Rev. C **85**, 054319 (2012).
[49] H. Jiang *et al.*, Phys. Rev. C **86**, 054304 (2012).
[50] T. Bäck, C. Qi, B. Cederwall, R. Liotta, F. Ghazi Moradi, A. Johnson, R. Wyss, and R. Wadsworth, Phys. Rev. C **87**, 031306(R) (2013).
[51] H. Jiang, Y. Lei, C. Qi, R. Liotta, R. Wyss, and Y. M. Zhao, Phys. Rev. C **89**, 014320 (2014).
[52] L. Coraggio *et al.*, Phys. Rev. C **91**, 041301(R) (2015).
[53] A. P. Zuker, Phys. Rev. C **103**, 024322 (2021).
[54] M. J. G. Borge and K. Riisager, Eur. Phys. J. A **52**, 334 (2016).
[55] N. Warr *et al.*, Eur. Phys. J. A **49**, 40 (2013).
[56] V. Fedosseev, K. Chrysalidis, T. D. Goodacre, B. Marsh, S. Rothe, C. Seiffert, and K. Wendt, J. Phys. G **44**, 084006 (2017).
[57] D. Cline, Annu. Rev. Nucl. Part. Sci. **36**, 683 (1986).
[58] A. N. Ostrowski, S. Cherubini, T. Davinson, D. Groombridge, A. M. Laird, A. Musumarra, A. Ninane, A. di Pietro, A. C. Shotter, and P. J. Woods, Nucl. Instrum. Methods Phys. Res., Sect. A **480**, 448 (2002).
[59] T. Czosnyka, D. Cline, and C. Y. Wu, Bull. Am. Phys. Soc. **28**, 745 (1983).
[60] K. Alder and A. Winther, Rev. Mod. Phys. **28**, 432 (1956).
[61] K. Alder and A. Winther, *Coulomb Excitation: A Collection of Reprints* (Academic, New York, 1966).
[62] K. Alder and A. Winther, *Electromagnetic Excitation: Theory of Coulomb Excitation with Heavy Ions* (North-Holland, Amsterdam, 1975).
[63] M. Zielińska, L. P. Gaffney, K. Wrzosek-Lipska, E. Clément, T. Grahn, N. Kesteloot, P. Napiorkowski, J. Pakarinen, P. Van Duppen, and N. Warr, Eur. Phys. J. A **52**, 99 (2016).
[64] N. Kesteloot *et al.*, Phys. Rev. C **92**, 054301 (2015).
[65] M. Klintefjord *et al.*, Phys. Rev. C **93**, 054303 (2016).
[66] A. Illana *et al.*, Phys. Rev. C **108**, 044305 (2023).
[67] S. Agostinelli *et al.*, Nucl. Instrum. Methods Phys. Res., Sect. A **506**, 250 (2003).
[68] J. Allison *et al.*, IEEE Trans. Nucl. Sci. **53**, 270 (2006).
[69] J. Allison *et al.*, Nucl. Instrum. Methods Phys. Res., Sect. A **835**, 186 (2016).
[70] Y. Tsunoda (private communication).
[71] A. Blazhev (private communication).
[72] D. T. Yordanov *et al.*, Phys. Rev. C **98**, 011303(R) (2018).
[73] B. J. Coombes *et al.*, Phys. Rev. C **100**, 024322 (2019).
[74] J. Park *et al.*, Phys. Rev. C **102**, 014304 (2020).
[75] H. Grawe *et al.*, Phys. Lett. B **820**, 136591 (2021).
[76] T. J. Gray *et al.*, Phys. Lett. B **847**, 138268 (2023).
[77] O. Kavatsyuk *et al.*, Eur. Phys. J. A **31**, 319 (2007).
[78] T. Faestermann, M. Górska, and H. Grawe, Prog. Part. Nucl. Phys. **69**, 85 (2013).
[79] S. Bogner, T. T. S. Kuo, and A. Schwenk, Phys. Rep. **386**, 1 (2003).
[80] D. R. Entem and R. Machleidt, Phys. Lett. B **524**, 93 (2002).
[81] J. Duflo and A. P. Zuker, Phys. Rev. C **59**, R2347 (1999).
[82] M. Dufour and A. P. Zuker, Phys. Rev. C **54**, 1641 (1996).
[83] E. Caurier, G. Martínez-Pinedo, F. Nowacki, A. Poves, and A. P. Zuker, Rev. Mod. Phys. **77**, 427 (2005).
[84] T. Otsuka, M. Honma, T. Mizusaki, N. Shimizu, and Y. Utsuno, Prog. Part. Nucl. Phys. **47**, 319 (2001).
[85] N. Shimizu *et al.*, Prog. Theor. Exp. Phys. **2012**, 01A205 (2012).
[86] M. Honma, T. Otsuka, T. Mizusaki, and M. Hjorth-Jensen, Phys. Rev. C **80**, 064323 (2009).
[87] M. Honma *et al.*, RIKEN Accel. Prog. Rep. **45**, 35 (2012).
[88] B. Fogelberg, M. Hellström, D. Jerrestam, H. Mach, J. Blomqvist, A. Kerek, L. O. Norlin, and J. P. Omtvedt, Phys. Rev. Lett. **73**, 2413 (1994).
[89] G. J. Feldman and R. D. Cousins, Phys. Rev. D **57**, 3873 (1998).
[90] G. Bruge, J. C. Faivre, H. Faraggi, and A. Bussiere, Nucl. Phys. **A146**, 597 (1970).
[91] F. G. Kondev, Nucl. Data Sheets **109**, 1527 (2008).
[92] J. L. Quebert, K. Nakai, R. M. Diamond, and F. S. Stephens, Nucl. Phys. **A150**, 68 (1970).
[93] D. Ralet *et al.*, Phys. Lett. B **797**, 134797 (2019).
[94] J. C. Hardy and I. S. Towner, Phys. Rev. C **71**, 055501 (2005).
[95] A. M. R. Joye, A. M. Baxter, S. Hinds, D. C. Kean, and R. H. Spear, Phys. Lett. B **72**, 307 (1978).
[96] J. F. Ziegler, M. D. Ziegler, and J. P. Biersack, Nucl. Instrum. Methods Phys. Res., Sect. B **268**, 1818 (2010).

End Matter

Concerning the closeness in energy between the 1243-keV γ ray from the 4_2^+ state and the 1246-keV γ ray from the 3_1^- state, the 3_1^- state is known to decay also by a 262-keV γ ray to the 4_1^+ state with a branching ratio of 40(4)% relative to the 1246-keV transition at 100(13)%. Accounting for the Miniball efficiencies and internal conversion coefficients, the expected number of detected counts of the 262-keV γ ray for every 1246-keV γ ray is 1.07(18). If gated on the 1212-keV γ ray and assuming all of the counts at the 1243-keV peak correspond to the 1246-keV γ ray from the 3_1^- state, the expected number of 262-keV γ ray is 15(5) counts. In the γ-ray single spectrum, 340(60) counts are expected at the 262-keV peak. No discernible peak was found at 262 keV in neither the singles (see Fig. 1) nor the γ-γ coincidence projection spectra. The 2σ upper limit on the singles intensity of the 262-keV γ ray was deduced to be 200 counts, following the Feldman-Cousins

approach for small signals in the presence of known background [89]. Although a small fraction of the counts associated with the 1243-keV transition could be associated with the 1246-keV γ ray from the 3_1^- state, no tangible evidence of Coulomb excitation to the 3_1^- state was found in this experiment. Nevertheless, the 2σ upper limit for the 262-keV γ-ray intensity could be inferred using the spectrum shown in the inset in Fig. 1 and applied in the Coulomb excitation analysis described above. This hypothetical scenario would imply that the intensity of the γ ray from the 4_2^+ state would be reduced by 58%, leading to the reduction of the $\langle 2_1^+||E2||4_2^+\rangle$ matrix elements in Table II by 32% and, correspondingly, the $B(E2;4_2^+ \rightarrow 2_1^+)$ value by 54% in Table III. In the same scenario, the $B(E2;2_1^+ \rightarrow 0_1^+)$ and $Q(2_1^+)$ values would increase by $\sim 0.5\sigma$, while the $B(E2;4_1^+ \rightarrow 2_1^+)$ value would decrease by $\sim 0.5\sigma$ relative to the results listed in Table III. The main results concerning $B(E2)$ and $Q(2_1^+)$ of this Letter would remain unchanged. Under the same hypothesis, $B(E3\downarrow) < 1.6 \times 10^4$ e^3 fm^6 was derived. The corresponding $B(E3\uparrow) < 0.11$ e^3 b^3 value agrees with the experimental $B(E3\uparrow)$ literature in the neighboring isotope ^{112}Sn: 0.087(12) e^3 b^3 [11] and 0.05(1) e^3 b^3 [90].

The full width at half-maximum (FWHM) of the 985-keV γ ray was approximately 15 keV. On the other hand, the FWHM of the 1243-keV γ ray was about 30 keV, slightly greater then 23 keV observed for the FWHM of the main 1212-keV γ ray. The different widths of the γ-ray peaks reflect the different half-lives of the 4^+ states and the distribution of scattering angles of ^{110}Sn, which influence the kinematics of ^{110}Sn inside the ^{206}Pb target and consequently the Doppler shift profile of the deexcitation γ rays.

Significant care was taken to include known error sources in the analysis. The uncertainty associated with the silicon detector distance from the target was 0.4 mm from fitting the isotropic distribution of alpha particles from the calibration source to the detected intensities in the different annular strips of the silicon detector, including a scale factor to account for absolute intensities. This results in 1% variations in the angular ranges of each ring strip. The systematic uncertainty of the γ-ray detection efficiency of Miniball was derived as 2.3% between 800 and 1300 keV, by Monte Carlo simulations of the efficiency curve parameters and evaluating the χ^2 values against the measured γ-ray efficiencies. Care was also taken when adopting the literature values of $\langle 0_1^+||E2||2_1^+\rangle$ and $\langle 2_1^+||E2||2_1^+\rangle$ of ^{206}Pb to be used for normalization of the γ-ray yields of ^{110}Sn. The evaluated $B(E2;0_1^+ \rightarrow 2_1^+)$ value from Coulomb excitation and inelastic scattering experiments is 0.101(3) e^{2}b^2 [91]. The inclusion of two previous half-life measurements [92,93] and the half-life ($T_{1/2}$) extracted for the 2_1^+ state in ^{206}Pb in this Letter gives a $B(E2;0_1^+ \rightarrow 2_1^+) = 0.0905(51)$ e^2 b^2 in ^{206}Pb. In order to accommodate the $\sim 2\sigma$ difference in $B(E2)$ values between measurements in ^{206}Pb, the uncertainty associated with the weighted average of the two values was increased according to the procedure outlined in Ref. [94]. The final $B(E2)$ value used for the target normalization in the iterative analysis was 0.0985(46) e^2 b^2. The $\langle 2_1^+||E2||2_1^+\rangle$ value of ^{206}Pb was set as 6.6(12) efm^2 [$Q(2_1^+) = 5(9)$ efm^2], from Ref. [95].

The uncertainty associated with the ^{110}Sn beam energy is gauged to be 0.5%, according to the spread in deviations of the centroid beam energies for the different accelerated beams at HIE-ISOLDE around this experiment. After applying 1σ shifts for the beam energy in the GOSIA analysis, the $B(E2)$ values for all states in ^{110}Sn deviated by less than 1%, and the $Q(2_1^+)$ value varied by 3.6% compared to the values stated in the main text. The Coulomb excitation target was ^{206}Pb, which was produced at GSI by rolling the ^{206}Pb sheet in air between stainless steel. The mass of the ^{206}Pb sheet was then measured by a balance, followed by area measurements to determine the areal density as 4 mg/cm^2. The accuracy of the thickness was within 1%, as the balance which measured the target mass possessed an accuracy of a few micrograms. The largest source of error was associated with the area of the ^{206}Pb sheet which was then cut for the target, but its relative uncertainty was effectively reduced by large dimensions. The 1% variation in thickness of the target for the GOSIA analysis corresponds to a $\sim$0.5% uncertainty in the mean energy of the beam at the center of the target (half thickness). This magnitude is identical to the experimental uncertainty on the beam energy for the GOSIA analysis; thus, the uncertainties on $B(E2)$ and $Q(2_1^+)$ from the target thickness are $< 1\%$ and 3.6%, respectively. These systematic uncertainties were added to the statistical counterparts in quadrature in the final results, but their contributions were negligible.

In the following, we give further details for the two analysis methods, i.e., the iterative method [63] that uses the known $B(E2)$ in ^{206}Pb for absolute normalization and the DSAM approach that uses the extracted half-life for the 2_1^+ state in ^{110}Sn for the same purpose.

In the iterative approach, the χ^2 plane spanned by the transitional matrix element $\langle 0_1^+||E2||2_1^+\rangle$ and the diagonal matrix element $\langle 2_1^+||E2||2_1^+\rangle$ was scanned by evaluating the χ^2 value between the observed and calculated γ-ray intensities using the Coulomb excitation code. In the first step, the known $B(E2;2_1^+ \rightarrow 0_1^+)$ value and the measured $2_1^+ \rightarrow 0_1^+$ transition intensity in ^{206}Pb are used for overall normalization in GOSIA2, which is a special version of GOSIA that enables simultaneous normalization of the γ-ray yields of the beam and the target nuclei during the minimization step. The $(\langle 2_1^+||E2||2_1^+\rangle, \langle 0_1^+||E2||2_1^+\rangle)$ pair for ^{110}Sn that gives the smallest χ^2 in the scan is then used in

a second step, where also the transitional matrix elements $\langle 2_1^+||E2||4_1^+\rangle$ and $\langle 2_1^+||E2||4_2^+\rangle$ are minimized together with $\langle 2_1^+||E2||2_1^+\rangle$, now introducing the $\langle 0_1^+||E2||2_1^+\rangle$ value of ^{110}Sn as an absolute normalization for the standard GOSIA calculations. It is declared together with its uncertainty as an additional data point. The matrix elements of ^{206}Pb are not involved in the second step, where standard GOSIA is used. This procedure is due to the design of the Coulomb excitation code and is needed to maintain correct normalization and error propagation. The new set of matrix elements is thereafter used for a new scan of the $(\langle 2_1^+||E2||2_1^+\rangle,\langle 0_1^+||E2||2_1^+\rangle)$ χ^2 surface in the third step using GOSIA2, and the procedure is iterated until a converged set of $(\langle 2_1^+||E2||2_1^+\rangle,\langle 0_1^+||E2||2_1^+\rangle)$ values is obtained. The convergence criterion was defined as an absolute difference of ≤ 0.1 efm^2 between successive iteration steps for the $\langle 0_1^+||E2||2_1^+\rangle$ matrix element. The error bars for the points in Fig. 3 include correlations of $\langle 2_1^+||E2||4_1^+\rangle$ and $\langle 2_1^+||E2||4_2^+\rangle$. The isomeric 6_1^+ buffer state with its half-life of 5.6(3) ns was included in the standard GOSIA minimization stages, to account for possible excitation of higher-lying states.

For the DSAM approach, a dedicated γ-ray line shape simulation was developed in Geant4 [67–69] in order to determine the relevant half-lives. The geometry of the experimental setup was constructed in Geant4, and γ-ray emission from the observed excited states was simulated for different half-lives as the nuclei were propagated through the target. A beam spot size of 1 mm in Gaussian σ was simulated. Stopping powers of ^{110}Sn and ^{206}Pb ions in the target were calculated with the SRIM software [96]. The χ^2 between the observed and simulated spectra was used to find the optimal half-lives. The 1σ statistical uncertainties to the best-fit $T_{1/2}$ value was derived from the lower and upper range in the trial $T_{1/2}$, using $\chi^2 = \chi^2_{\rm min} + 1$. A 10% systematic uncertainty on the final $T_{1/2}$ was added, originating from uncertainties in the beam energy, stopping power of ^{206}Pb calculated by SRIM, the thickness of the Coulomb excitation target, inaccuracies in the simulated geometry, and γ-ray efficiency compared to the true experimental values. As a proof of principle, the half-life of the 2_1^+ state in ^{206}Pb was determined using the simulation to be $T_{1/2}(2_1^+) = 9.8^{+2.8}_{-2.1}$ ps, which is consistent with the literature values of 9.1(6) [92] and 12(3) ps [93]. This result provides support for the soundness of the $T_{1/2}$ values obtained for ^{110}Sn. One should note that, for proper analysis, delayed feeding to the 2_1^+ state by the observed $4_{1,2}^+$ states needs to be taken into account. The 985-keV γ ray from the 4_1^+ state contained enough statistics for its own $T_{1/2}$ determination, but the weak 1243-keV γ ray from the 4_2^+ state, which rides on the side of the Doppler-shifted 1212-keV line, could not be determined from the simulation. Therefore, the half-life of the 4_2^+ state was deduced from the $B(E2; 4_2^+ \rightarrow 2_1^+)$ value obtained from the GOSIA analysis. The equivalent $T_{1/2}$ of the 4_2^+ state is $\approx$0.7 ps. Several comparisons of the experimental and simulated γ-ray energy spectra, for χ^2 evaluations of the trial half-lives, are shown in Fig. 4. The horizontal arrows indicate the χ^2 evaluation regions for determining the half-lives of the 4_1^+ and 2_1^+ states in ^{110}Sn. The weighted residuals for each bin in the bottom panels in Fig. 4 represent $\sigma = (N_{\rm sim} - N_{\rm exp})/dN_{\rm exp}$, where N and dN are the counts and the uncertainties, respectively. The two-dimensional χ^2 surface, as a function of $T_{1/2}(2_1^+)$ and $T_{1/2}(4_1^+)$, is shown in Fig. 5. Contours of $\chi^2 \approx \chi^2_{\rm min} + 1.5$ (for clarity), $+2$, and $+3$ are drawn with solid, short-dashed, and long-dashed red lines, respectively. The influence of the variance on the half-life of the 4_2^+ state derived from the $B(E2)$ value determined from GOSIA was also tested via simulations. The half-lives of the 4_2^+ state corresponding to $\pm 1\sigma$ variations in $B(E2)$ are 0.5 and 1.4 ps, and simulated γ-ray line shape spectra stemming from these two values were incorporated in the $T_{1/2}$ analysis of the 2_1^+ and the 4_1^+ states. Compared to the values obtained with the nominal value of $T_{1/2}(4_2^+) = 0.7$ ps, differences up to 0.01 and 0.2 ps were observed for the best-fit half-lives of the 2_1^+ and the 4_1^+ states, respectively. The deviations are small and are included in the systematic uncertainties, as expected from the small contribution. The small magnitudes of fluctuations also provide a justification for treating the result based on the half-life normalization as largely independent from the result using the ^{206}Pb normalization for the combined result.